Electronic structure of CuGeO3 : charge excitations between zero and one dimension

Atzkern, S.; Knupfer, M.; Golden, M.S.; Fink, J.; Hübsch, A.; Waidacher, C.; Becker, K.W.; von der Linden, W.; Weiden, M.; Geibel, C.

Published in:
Physical Review B

Electronic structure of $CuGeO_3$: Charge excitations between zero and one dimension

S. Atzkern, M. Knupfer, M. S. Golden, and J. Fink
Institute for Solid State Research, IFW Dresden, P.O.Box 270016, D-01171 Dresden, Germany

A. Hübsch, C. Waidacher, and K. W. Becker
Institut für Theoretische Physik, Technische Universität Dresden, D-01062 Dresden, Germany

W. von der Linden
Institut für Theoretische Physik, Technische Universität Graz, Petersgasse 16, A-8010 Graz, Austria

M. Weiden and C. Geibel
Max-Planck-Institut für Chemische Physik fester Stoffe, D-01187 Dresden, Germany
(Received 2 March 2001; published 26 July 2001)

We present a joint experimental and theoretical investigation of the electronic structure of $CuGeO_3$. The momentum dependent loss function was measured using electron energy-loss spectroscopy in transmission. For momentum transfers parallel to the crystallographic **c** direction (along the CuO_2 chains) the loss function agrees well with calculations based upon a Cu_5O_{12} cluster model. The detailed analysis of the origin of the features below 7 eV in the calculated spectra reveals two distinct energy ranges in which transitions occur either into localized or delocalized states. A shift of spectral weight towards the low energy region can be observed when the coupling between adjacent CuO_4 plaquettes is increased in our model. Above 2 eV the optical conductivity derived from the experimental loss function agrees well with results from optical measurements as well as with those from calculations based on our cluster model. The small spectral weight observed at 1.8 eV in the experiment has no counterpart in the theoretical loss function and thus cannot be assigned to charge transfer transitions involving Cu and O states. The loss functions with momentum transfers parallel to the crystallographic **b** direction show spectral weight at 6.5 eV that shifts to higher energies with increasing momentum transfer. This can probably be ascribed to transitions involving unoccupied Ge 4*s* and 4*p* states.

DOI: 10.1103/PhysRevB.64.075112 PACS number(s): 71.27.+a

I. INTRODUCTION

In 1993 the discovery of the spin-Peierls (SP) transition in $CuGeO_3$ by Hase *et al.*[1] began a huge number of physical investigations of this compound. The SP transition in $CuGeO_3$ is the consequence of a dimerization of the Cu^{2+} ions aligned in CuO_2 chains below the transition temperature and has been intensively studied using neutron and x-ray diffraction.[2] The linear arrangement of the antiferromagnetically coupled Cu^{2+} ions provides an ideal system for the experimental examination of theoretical predictions made for a spin-1/2 Heisenberg chain.[3] Furthermore, $CuGeO_3$ belongs to the big group of low-dimensional cuprates which are under lively discussion due to their outstanding properties. The common structural unit of these materials is the square-planar CuO_4 plaquette, and it is interesting to see how the properties of the cuprates depend on the arrangement of the plaquettes in the crystal. As in the ''zero-dimensional'' compound Li_2CuO_2, in $CuGeO_3$ the CuO_4 plaquettes build edge-sharing CuO_2 chains. However, in contrast to Li_2CuO_2, the plaquettes show a more distinct rectangular distortion which gives rise to the assumption that the character of the electronic states in $CuGeO_3$ is rather one dimensional, due to the more pronounced superexchange path between adjacent Cu 3*d* orbitals. An estimation of the exchange interactions between the holes on the plaquettes[4] shows that such an elongation of the plaquettes along the CuO_2 chain direction is insufficient to transform the spin system from a ferromagnetic coupling to an antiferromagnetic coupling as described by the Goodenough-Kanamori-Anderson rules.[5] This is in contrast the experimental results, which found an antiferromagnetic alignment of the hole spins along the chain direction. As a solution of this discrepancy Geertsma and Khomskii[4] proposed an additional superexchange pathway via the Ge orbitals which hybridize with the 2*p* orbitals of the chain oxygens.

The electronic structure of $CuGeO_3$ has been intensively studied theoretically by means of band structure[6–8] and cluster calculations[9] as well as experimentally using different spectroscopic methods.[10–14] Even though the results of the band structure calculations show contributions of the Ge states to the conduction band, the influence of these states as regards the dynamics of the 3*d* holes in $CuGeO_3$ could not yet be determined experimentally. In this respect, the investigation of the valence band excitations should be able to provide more information. However, contradictory results from optical measurements[10–12] have made a reliable interpretation of the charge excitations in the visible energy range difficult.

In order to overcome this weakness, we present a joint experimental and theoretical investigation of the valence band excitations and their momentum dependence in $CuGeO_3$ using high resolution electron energy-loss spectroscopy (EELS) in transmission and Cu_5O_{12} cluster calculations

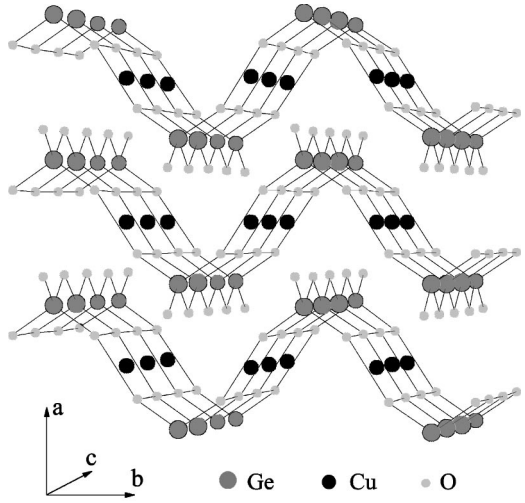

FIG. 1. Crystal structure of $CuGeO_3$. Copper atoms are shown as black spheres, oxygen atoms as light grey spheres, and germanium atoms as dark grey spheres.

based on a multiband Hubbard model. The comparison of the experimental and theoretical data allows us to distinguish between transitions into localized and delocalized final states which provides us with detailed information about the electronic structure in this compound. In a more general way, from the variation of the interplaquette coupling in our theoretical model we can draw conclusions regarding the change of the dynamics of the holes in a CuO_2 chain with the transition from zero to one dimension. The differences between the theoretical and the experimental results determined with momentum transfer parallel to the crystallographic **b** direction gives us useful information about the possible contributions of the Ge states to the conduction band.

II. EXPERIMENT

A. Samples

For the growth of the $CuGeO_3$ single crystals, a $CuGeO_3$ melt with an excess of 20 wt. % CuO was slowly cooled down from 1200 ° C at a rate of 2 C/h in a Pt crucible. The single crystals—blue platelets with dimensions of 1.5 mm $\times$5 mm$\times$4 mm along the **a**, **b**, and **c** axis—respectively, could easily be separated from the remaining CuO flux. The quality of the single crystals was investigated by means of susceptibility measurements using a commercial SQUID (MPMS) system. A well-defined spin-Peierls transition at 14.6 K as well as a negligible Curie contribution at low temperatures indicated the high quality of these flux-grown single crystals.

Figure 1 shows the crystal structure of $CuGeO_3$.[15] The Cu atoms and their four neighboring O atoms build chains of edge-sharing CuO_4 plaquettes along the crystallographic **c** direction with a Cu-O-Cu-bond angle of almost 98°. Along the **b** direction the plaquettes of adjacent chains are tilted out of the *ac* plane in such a way as their perpendiculars intersect with an angle of around 112°. The Ge atoms are tetrahedrally surrounded by O atoms. In the **b** direction these tetrahedra connect adjacent chains leading to a wavelike $CuGeO_3$ network as illustrated in Fig. 1. These networks are stacked along the **a** direction. The weak interactions between them are the reason for the excellent cleavage behavior parallel to the *bc* plane. The distance between the Cu atom and the O atoms of a plaquette is 1.94 Å, while the distance between the Ge atoms and the nearest neighbor O atoms of the plaquettes is much smaller (1.72 Å).

For the measurements using electron energy-loss spectroscopy in transmission, a thin slice was peeled off the single crystal using an adhesive tape. This slice was further cleaved by repeated peeling with tape stripes, providing a final thin film thickness of about 1000 Å. The remaining tape glue was subsequently dissolved in chloroform. The high quality and orientation of the single crystalline samples were checked by *in situ* electron diffraction.

B. EELS in transmission

EELS in transmission with a primary beam energy of 170 keV was performed on free standing films at room temperature (for experimental details see Ref. 16). The energy and momentum transfer (q) resolution were chosen to be 200 meV and 0.03 $Å^{-1}$ for $q < 0.4$ $Å^{-1}$, and 300 meV and 0.05 $Å^{-1}$ for $q \geqslant 0.4$ $Å^{-1}$, in order to compensate for the decrease of the cross section at higher momentum transfer.

EELS in transmission provides us with the momentum and energy dependent loss function $\mathrm{Im}[-1/\varepsilon(\mathbf{q},\omega)]$, from which, by means of the Kramers-Kronig relations, the real part of the negative inverse dielectric function and thus all the optical properties such as, for example, the optical conductivity $\sigma(\mathbf{q},\omega)$ can be calculated. For small momentum transfer only dipole transitions are allowed, and for the limit $q=0$ the transition matrix elements are the same as in optics. For the Kramers-Kronig analysis (KKA), a loss spectrum close to the optical limit was used in order to derive the optical conductivity. The measured data have been corrected for contributions from the quasielastic line and multiple scattering processes.[16] The KKA was normalized using the refractive index (see below).

III. THEORY

The loss function $L(\mathbf{q},\omega)$ measured in EELS experiments is given by

$$L(\mathbf{q},\omega) \equiv \mathrm{Im}\left[\frac{-1}{\epsilon(\mathbf{q},\omega)}\right] \sim \frac{1}{\mathbf{q}^2}\,\mathrm{Im}\,\chi_\rho(\mathbf{q},\omega),$$

where the prefactor $1/\mathbf{q}^2$ is due to the Coulomb interaction between the scattered electrons and the electrons of the sample.[16,17] $\chi_\rho(\mathbf{q},\omega)$ is the **q**- and ω-dependent dynamic density-density correlation function of the sample including long-range Coulomb interactions. By treating the latter within the random-phase approximation (RPA), one finds for the loss function (see also Ref. 18)

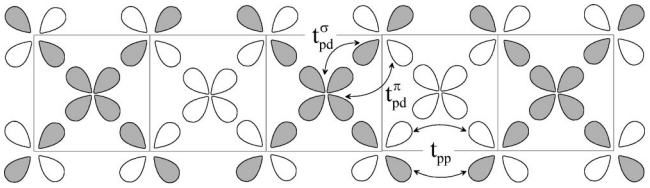

FIG. 2. Cu_5O_{12} cluster used in the calculations of the loss functions and the optical conductivity of $CuGeO_3$. In the model only the Cu $3d_{x^2-y^2}$ and O $2p_{x(y)}$ orbitals are taken into account. The cluster is divided into two sublattices each marked by either shaded or unshaded orbitals. The definition of the hopping amplitudes t_{pd}^{σ}, t_{pd}^{π} and t_{pp} is symbolically given by the double arrows. See text for details.

$$L(\mathbf{q},\omega)\sim \mathrm{Im}\left[\frac{-1}{1+v_{\mathbf{q}}\chi_{\rho}^{0}(\mathbf{q},\omega)}\right], \tag{1}$$

where

$$\chi_{\rho}^{0}(\mathbf{q},\omega)=\frac{i}{\hbar}\int_{0}^{\infty}dt\langle 0|[\rho_{\mathbf{q}}(t),\rho_{-\mathbf{q}}]|0\rangle e^{i\omega t} \tag{2}$$

is the response function at zero temperature for a short-range interaction model. $|0\rangle$ is the ground state, $\rho_{\mathbf{q}}$ denotes the Fourier transform of the hole occupation number operator, and $v_{\mathbf{q}}=e^2N/(\epsilon_0\epsilon_r v\mathbf{q}^2)$ is the long-range Coulomb potential with unit cell volume v. Furthermore, N is the number of holes per unit cell, ϵ_0 is the permittivity, and ϵ_r is the static dielectric constant, i.e., the zero-frequency limit of $\epsilon_1(\omega)$. We note that the inclusion of the long-range Coulomb interaction means that the Coulomb interaction used in the short-range model below represents the unscreened value. This effect however is negligible in the case of the on-site Coulomb interaction U, which is considered below only.[19]

We evaluated Eqs. (1) and (2) by direct diagonalization using the standard Lanczos algorithm and a continued fraction expansion.[20] As the Lanczos method is limited to small clusters, we studied a system consisting of five edge-sharing CuO_4 plaquettes illustrated in Fig. 2 using open boundary conditions. We have checked the convergence of the calculated spectra with respect to the system size by compairing them with results from calculations based on a smaller system consisting of four plaquettes. In the undoped case, each of the CuO_4 plaquettes is occupied by a single hole with an antiferromagnetic spin alignment along the chain. Band structure calculations[6–8] provide us with the information that the bands straddling the chemical potential are mainly composed of Cu $3d_{x^2-y^2}$ and O $2p_{x(y)}$ states with predominantly Cu $3d_{x^2-y^2}$ character of the highest occupied band. Hence, our model is restricted to these orbitals. For reasons which will become clear in the following we divided the Cu_5O_{12} cluster into two sublattices. The first of them contains three Cu sites and those O $2p$ orbitals which show the strongest overlap with the three Cu $3d_{x^2-y^2}$ orbitals (these orbitals are shaded gray in Fig. 2). The second sub-lattice contains two Cu sites and the remaining O $2p$ orbitals (unshaded orbitals in Fig. 2). Therefore, the studied Cu_5O_{12} cluster shown in Fig. 2 contains five holes, and consists of five Cu $3d_{x^2-y^2}$ orbitals and twelve O sites with two $2p$ orbitals per site. This leads to a Hilbert space with 1 483 524 basis states. For the calculation of the loss functions we used a one-dimensional extended multiband Hubbard model at half-filling (one hole per Cu site). In the hole picture the corresponding Hamiltonian reads

$$\begin{aligned}H=&U\sum_{i\alpha}n_{i\uparrow}^{d\alpha}n_{i\downarrow}^{d\alpha}+\Delta\sum_{js\alpha}n_{js}^{p\alpha}+t_{pd}^{\sigma}\sum_{\langle ij\rangle s\alpha}\phi_{pd}^{ij}(p_{js}^{\alpha\dagger}d_{is}^{\alpha}+\mathrm{H.c.})\\&+t_{pd}^{\pi}\sum_{\substack{\langle ij\rangle s\\ \alpha\neq\beta}}\phi_{pd}^{ij}(p_{js}^{\alpha\dagger}d_{is}^{\beta}+\mathrm{H.c.})\\&+t_{pp}\sum_{\langle jj'\rangle s\alpha}\phi_{pp}^{jj'}(p_{js}^{\alpha\dagger}p_{j's}^{\alpha}+\mathrm{H.c.}).\end{aligned} \tag{3}$$

The operators $d_{is}^{\dagger}(p_{js}^{\dagger})$ create a hole with spin s in the ith Cu $3d$ orbital (jth O $2p$ orbital). The n_{is}^{d} ($n_{js}^{p\alpha}$) are the corresponding number operators. The operators for the different sublattices are labeled by the superscripts α and β. The prefactors ϕ_{pd}^{ij} and $\phi_{pp}^{jj'}$ provide the correct sign for the hopping processes, and $\langle ij\rangle$ denotes the summation over nearest neighbor pairs.

The hopping parameters t are defined in Fig. 2. In order to minimize the number of model parameters we chose only a single hopping parameter t_{pp} to describe the hopping between neighboring O $2p$ orbitals belonging to the same sublattice. Thus we neglect the hopping between neighboring O $2p$ orbitals belonging to different sublattices. As a further simplification, we use the same t_{pp} value for the hopping in the chain direction as well as perpendicular to it. This approximation is justified by additional calculations which showed that an anisotropy in the O-O hopping would only cause a shift of the energy scale and thus can be absorbed into a renormalized charge-transfer energy Δ without affecting the spectra.

As for the hopping between the copper and the oxygen orbitals, we distinguish between two hopping parameters. The hopping amplitude t_{pd}^{σ} describes the intraplaquette hopping between a Cu $3d_{x^2-y^2}$ and an adjacent O $2p$ orbital of the same sublattice. For Cu-O-Cu bond angles with a small deviation from 90° the bond between these orbitals has mainly σ character. The parameter t_{pd}^{π} denotes the hopping between the predominantly π bonding Cu $3d_{x^2-y^2}$ and O $2p$ orbitals of different sublattices. We would like to emphasize that in our model only a finite value of t_{pd}^{π} allows the hopping between the two sublattices and consequently describes the charge transfer to the nearest neighbor (NN) plaquette.

Each of the hopping amplitudes t_{pd}^{σ} and t_{pd}^{π} can be expressed by a linear combination of the two-center integrals $(pd\sigma)$ and $(pd\pi)$, given by Slater and Koster.[21] The corresponding coefficients are a function of the direction cosines of the vector that points from the Cu atom to the O atom. If we apply the common approximation $(pd\pi)\simeq -0.5(pd\sigma)$,[22] the Slater-Koster integrals provide us with the simple relation $t_{pd}^{\pi}=-x\cdot t_{pd}^{\sigma}$ with the interplaquette coupling constant x being determined by the geometry. For our cluster

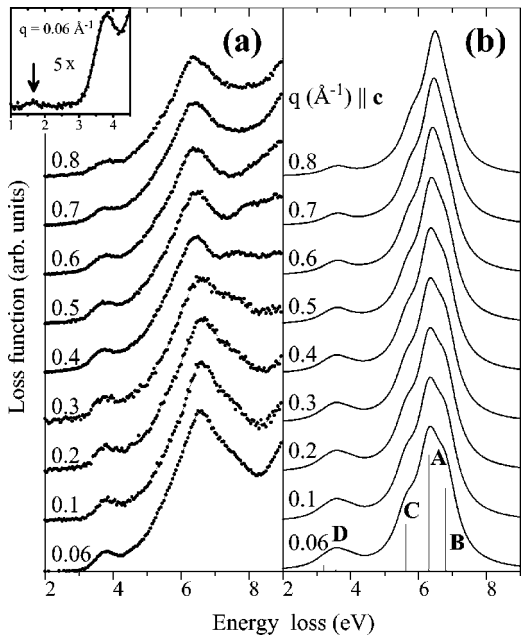

FIG. 3. The loss functions of $CuGeO_3$ (a) measured using EELS in transmission with momentum transfer aligned along the crystallographic **c** direction and (b) calculated using a one-dimensional extended multiband Hubbard model at half filling. The inset shows the fivefold magnified experimental spectrum below 4.5 eV measured with $\mathbf{q}=0.06$ Å^{-1}.

as shown in Fig. 2, x is a function of the Cu-O-Cu-bond angle and thus represents an additional parameter which allows us to study in a more general way the influence on the theoretical spectra of an increase in the rectangular distortion $(x\rightarrow 1)$ of the square $(x=0)$ CuO_4 plaquettes. In $CuGeO_3$ the Cu-O-Cu-bond angle is 98° which corresponds to $x=0.17$.

Consequently, there remain four independent parameters in our theoretical model whose values we chose as follows. For U we took 8.8 eV, a typical value for the on-site Coulomb interaction in cuprates.[23] The hopping parameter $t_{pd}^{\sigma}=1.1$ eV we calculated by means of the Slater-Koster relations using the two-center integrals determined for $CuGeO_3$ in Ref. 9. Finally, there are two free parameters: the charge transfer energy $\Delta=5.3$ eV and the hopping parameter $t_{pp}=0.4$ eV, which have been adjusted to obtain the correct peak position with respect to the experimental loss functions. The value of Δ is significantly larger than in other cuprates and can be explained by the larger difference in the Madelung site potential between the Cu and O sites in $CuGeO_3$.[9] As the normalization parameter for the RPA and the KKA we used a value of $\epsilon_r=4$ (see also below).

IV. RESULTS AND DISCUSSION

A. Loss function with q‖c

In Fig. 3(a) we show the EELS loss function of $CuGeO_3$ recorded for different values of **q** parallel to the crystallographic **c** direction. The spectra are normalized at higher energy (around 12 eV) where the shape of the spectra does not change with the value of the momentum transfer. For clarity the spectra are incrementally off-set in the y direction.

The loss functions are dominated by two features: an intense peak with triangularlike shape at 6.2 eV and a feature with much lower intensity at 3.5 eV. The peak positions of both features do not change with increasing momentum transfer, whereas their intensity decreases at higher **q**. In contrast, the intensity of a shoulder at 7.5 eV increases with increasing **q**, passes through a maximum at 0.4 Å^{-1} and vanishes above 0.5 Å^{-1}. A second shoulder at 8 eV shows a quite similar behavior with a maximum at 0.5 Å^{-1}. Since in electron energy-loss spectroscopy the cross section for dipole transitions decreases and that for dipole-forbidden transitions increases with increasing momentum transfer, we can infer that the main features at 3.5 and 6.2 eV are related to dipole transitions whereas the shoulders above 7 eV have their origin in monopole or quadrupole transitions. As the inset of Fig. 3(a) shows, an additional peak—whose weak intensity does not change significantly with increasing **q** (not shown)—is seen in the loss function of $CuGeO_3$ at about 1.7 eV. This peak can most probably be assigned to the same transitions which are responsible for the peak at ~ 1.8 eV in the optical conductivity derived from optical measurements[10–12] and a peak at 1.7 eV observed in EELS in reflection measurements.[24] In the literature the origin of these low-energy transitions is discussed controversially. On the one hand they are assigned to charge transfer excitations between O $2p$ and Cu $3d$ states[10,12] while, on the other hand, they were attributed to phonon-assisted d-d transitions between crystal field split Cu $3d$ levels.[11,24]

In order to find out which excitations contribute to the observed features we have calculated the loss functions as described in Sec. III. In Fig. 3(b) the results of our cluster calculations for **q** parallel to the chain direction are shown. To allow a direct comparison with the experimental spectra [Fig. 3(a)], the calculated data were broadened with a Gaussian function of 0.4 eV width. The broadened theoretical curves in Fig. 3(b) have been scaled to match the maximum of the intensity of the 6.2 eV feature for $\mathbf{q}=0.4$ Å^{-1} in the experimental data. However, the differences in intensity the cluster results for higher and lower **q** are a valid result of the calculations. The unbroadened spectrum for $\mathbf{q}=0.06$ Å^{-1} is also shown as vertical lines in Fig. 3(b).

The comparison of the experimental and theoretical loss functions in Fig. 3 shows that the energy positions as well as the shapes of the two main features at 3.5 and 6.2 eV are well reproduced by the calculations. Furthermore, the intensity ratio of these two features is also well described even though at high momentum transfer ($\mathbf{q}>0.5$ Å^{-1}) the intensity of the 6.2 eV feature seems to be smaller in the experimental loss functions. This stronger decrease of the peak height with increasing **q** in the experimental spectra probably can be ascribed to multiple scattering processes becoming more important at high momentum transfers. As generally observed in EELS spectra, the occurence of multiple scattering leads to an additional unstructured, decreasing background resulting in a decrease of the absolute maximum of

the peaks. The fact that below 7 eV the loss function of $CuGeO_3$ with momentum transfer parallel to the **c** direction can be fully described by interband excitations (i.e., interband plasmons[16]) which are related to transitions between hybridized Cu $3d_{x^2-y^2}$ and O $2p_{x(y)}$ states confirms our initial assumption that other states contribute only weakly to the band structure along the chain direction in this energy range. However, as Fig. 3 shows, this assumption does not hold for higher energies. It is clearly visible that in the theoretical loss functions the spectral weight at energy losses above 7 eV quickly drops to zero whereas in the experimental spectra several weak features can be observed. Thus the features above 7 eV can be assigned to transitions that involve states which are not contained in our model [e.g., Cu $4s$, Ge $4s(p)$]. In addition, below 2 eV no spectral weight appears in the theoretical loss functions. The absence of a peak in this energy region is compatible with the interpretation of the origin of the 1.8 eV feature in the experimental loss function [see inset of Fig. 3(a)] as phonon-assisted, intra-atomic Cu d-d transitions,[11,24] which are also not taken into account by our model.

The unbroadened spectrum in Fig. 3(b) illustrates that each of the two main peaks in the loss function is formed by a superposition of contributions from more than one excitation. In order to gain a deeper insight into the origin of the transitions contributing to the spectra we have analyzed the electronic states involved. The analysis of the ground state shows that about 72% of the hole density resides on the Cu site while the remaining 28% are spread over the nearest neighbor O $2p$ states. With respect to the final states, for the sake of clarity, we restrict ourselves to a mere qualitative description of the hopping of a single hole in a Cu_3O_8 cluster (Fig. 4) for which we have analyzed the excited states. Within this description, we single out one hole which in the ground state we suppose to be located on the central plaquette. The three different shades of the orbitals in Fig. 4 represent the probabilities for the considered hole to occupy the neighboring sites in the final states. Black color stands for high, gray color for medium, and white color for low hole density after the hopping process. For the calculation of the shown probabilities we have assumed that the Cu site of the central plaquette is unoccupied.

First, we focus on the three final states contributing to the 6.2 eV feature in the loss function [see the vertical lines A, B, and C in Fig. 3(b)]. The contribution with the highest intensity at 6.2 eV (peak A) has its origin in a charge transfer transition from the ground state into a localized final state with almost pure oxygen character [Fig. 4(a)]. This transition is the equivalent to the intraplaquette transition observed in the quasi-zero-dimensional compound Li_2CuO_2 at 4.8 eV.[9,25] In $CuGeO_3$ the corresponding plasmon is centred at 1.5 eV higher in energy due to the larger charge transfer energy in the germanium cuprate than in Li_2CuO_2. The plasmon at 6.8 eV (peak B) is related to a transition into a state which differs from A mainly by the presence of additional hole density on the O $2p_{x(y)}$ orbitals of the neighboring plaquette, which belongs to the second sublattice [Fig. 4(b)]. As was the case for final state A, final state B is also strongly localized due to the attractive interaction between the hole and the remaining

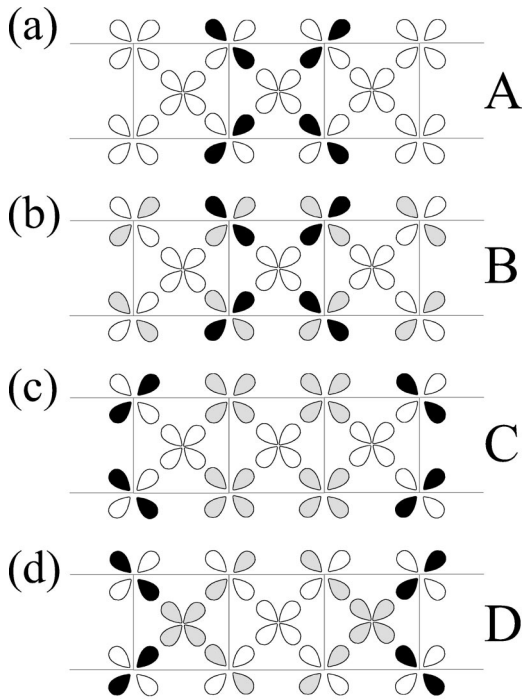

FIG. 4. Qualitative description of the four different final states A, B, C, and D [see Fig. 3(b)] of a single hole in a Cu_3O_8 cluster. The shades of the Cu $3d_{x^2-y^2}$ and O $2p_{x(y)}$ orbitals represent the probabilities $\langle n_j^{p\alpha}(1-n_{i\uparrow}^d)(1-n_{i\downarrow}^d)\rangle$ and $\langle n_{i'}^d(1-n_{i'\uparrow}^d)(1-n_{i'\downarrow}^d)\rangle$ of hole occupations at orbital α of O site j and at Cu site i' in the neighborhood of the central Cu site i which is assumed to be unoccupied ($n_{i'}^d=n_{i'\uparrow}^d+n_{i'\downarrow}^d, n_j^{p\alpha}=n_{j\uparrow}^{p\alpha}+n_{j\downarrow}^{p\alpha}$). The black, grey and white color stands for high, medium, and low hole density, respectively.

electron on the central plaquette. In contrast, the shoulder at 5.6 eV (peak C) can be assigned to the hopping of the hole to the oxygen orbitals of the next nearest neighbor (NNN) plaquette within the same sublattice [Fig. 4(c)] and thus can be regarded as a rather delocalized transition.

Finally, we turn to the feature between 3 and 5 eV (D). This feature is a superposition of plasmons related to transitions into delocalized states with enhanced occupation of orbitals on the NN and the NNN plaquettes. Since it is not possible to ascribe each peak in the unbroadened spectrum to a single transition, a characteristic final state hole distribution for the NN hopping is depicted schematically in Fig. 4(d). This state is characterized by a high hole density on the nearest neighbor plaquettes. The final state D corresponds to the formation of a spin singlet state on the neighboring plaquette—often called Zhang-Rice singlet[26]—which leads to the significantly lower excitation energy observed in the experimental spectra.

In order to distinguish the different contributions to the spectral weight of the low energy feature coming either from the NN or from the NNN hopping we varied the interplaquette coupling parameter x in the model. As the degree of delocalization is determined by x, its variation gives us information about the dependence of the theoretical loss function on the dynamics of the holes in the CuO_2 chain. From the geometrical point of view, by increasing x from 0

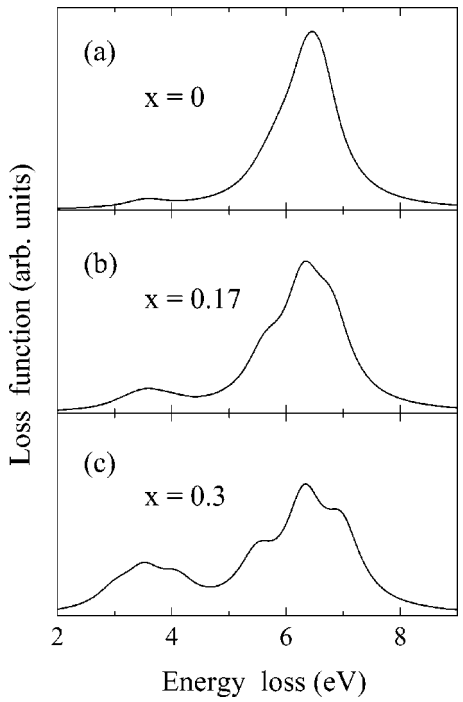

FIG. 5. The lines in (a), (b), and (c) show the calculated loss functions with $\mathbf{q}=0.06$ Å$^{-1}\|\mathbf{c}$ for the three different couplings $x=0$, $x=0.17$, and $x=0.3$ between the sublattices of the cluster, respectively. The cluster model and the definition of the coupling parameter x are described in the text.

to 1 we increase the Cu-O-Cu-bond angle from 90° to 180° thus simulating the gradual transition from a zero- to a one-dimensional system. In Fig. 5 the calculated loss functions with $\mathbf{q}=0.06$ Å^{-1} using three different values of x are shown. The on-site Coulomb interaction U, the charge transfer energy Δ as well as the hopping parameters t_{pd}^{σ} and t_{pp} were taken as described above. Starting from the loss function calculated with $x=0.17$, which corresponds to the spectrum of $CuGeO_3$ [see Fig. 5(b)], we have changed the parameter x in two opposite directions. On the one hand, we switched off the NN hopping by setting $x=0$, i.e., $t_{pd}^{\pi}=0$. The response seen in the loss function is a decrease of the spectral weight of the low energy peak [see Fig. 5(a)]. This behavior of the spectral weight below 4 eV allows two additional conclusions. First, the higher spectral weight at $x=0.17$ confirms that already with small deviations of the Cu-O-Cu-bond angle from 90° the NN hopping begins to contribute visibly to the loss function. Secondly, the nonvanishing spectral weight in the loss function with $x=0$ shows that the NNN hopping is not completely suppressed as one would expect for a ferromagnetic alignment of NNN spins in an antiferromagnetic spin-1/2 chain. This is a consequence of the deviations of the ground state spin structure from a simple antiferromagnetic arrangement for $x=0$. In this case the system decouples into two penetrated independent sublattices where every second Cu site belongs to the same sublattice (see Fig. 2). For each sublattice, in the ground state the holes are almost perfectly located on the Cu sites, and are antiferromagnetically ordered (↑-↓-↑). The nesting of the two sublattices shown in Fig. 2 results in antiferromagnetic aligned pairs of ferromagnetically coupled spins (↑↑↓↓↑). Only with increasing interaction between the sublattices ($x\rightarrow 1$) do the hole spins of the chain tend to align antiferromagnetically (↑↓↑↓↑). However, the rather weak interplaquette coupling in $CuGeO_3$ is not able to realign the spins completely leading to a strong frustration of the hole spins.

On the other hand, we increased the value of x up to 0.3 which corresponds to a Cu-O-Cu bond angle of about 105°. The result is shown in Fig. 5(c). It is striking that, in contrast to $x=0$, already such a small tilt of the Cu-O bond towards the chain axis substantially shifts the spectral weight from the energy range above 6 eV (dominated by transitions into localized states) to the feature around 3.5 eV (originating from transitions into delocalized states).

In order to complete our study as regards the variation of the interplaquette coupling parameter x we refer to similar experimental investigations of two compounds whose crystal structures allow a qualitative comparison with our findings. First, Li_2CuO_2 is a representative of a zero-dimensional system which also contains edge-sharing CuO_4 chains with a Cu-O-Cu-bond angle of 94°. Since the charge transfer energy in this compound ($\Delta=2.7$ eV) is much smaller than in $CuGeO_3$ a more quantitative comparison with our theoretical data can be made by shifting the energy scale in Fig. 5(a) by around 1.5 eV. In fact, EELS studies[25] as well as optical measurements[9] of Li_2CuO_2 show a single feature at about 4.5 eV which can be ascribed to intraplaquette excitations. However, no spectral weight can be observed around 2 eV where small but nonetheless visible contributions from transitions into delocalized states (NNN hopping) would be expected in this compound. The reason for this discrepancy most probably lies in the coupling of the hole spins along the chains. As explained above, in $CuGeO_3$ the spins are coupled antiferromagnetically along the chains with a strong frustration of the NNN spins. In contrast, in Li_2CuO_2 the ferromagnetic alignment of the spins due to the strong Hund's rule coupling[5] additionally suppresses the NN as well as the NNN hopping. Therefore, the loss function of Li_2CuO_2 is more comparable with that of an isolated plaquette. Secondly, a typical representative of a one-dimensional system with $x=1$ is Sr_2CuO_3 containing linear chains of corner-sharing plaquettes. Though in this case also only a qualitative comparison of the experimental data with the loss function in Fig. 5(c) is possible, the predicted shift of spectral weight to lower energies is confirmed by a feature with high intensity around 2 eV in the experimental loss function of Sr_2CuO_3.[19]

For a comparison of our data with the spectra obtained by optical measurements we have calculated the optical conductivity $\sigma_c(\mathbf{q},\omega)$ from the experimental loss function with momentum transfer $\mathbf{q}=0.08$ Å^{-1} by means of a KKA. The result of this analysis is shown in Fig. 6(a). In $\sigma_c(\mathbf{q},\omega)$ derived from the EELS spectrum the spectral weight below 2 eV is also very weak ($\epsilon_2<3\times10^{-2}$). This is in contrast to the much higher intensity ($\epsilon_2\simeq 10$) visible around 1.3 eV in reflectivity measurements[10] but coincides well with results from optical absorption measurements.[11] The discrepancy in the strength of this feature might either be related to the different kinds of interference characteristics for each mea-

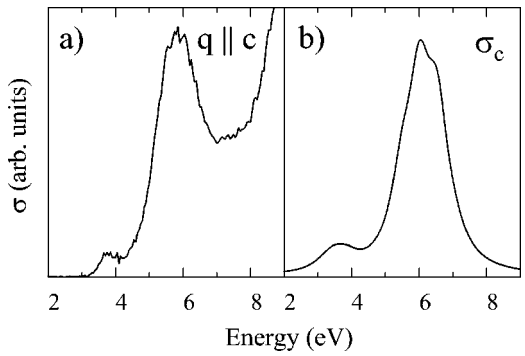

FIG. 6. The optical conductivity of $CuGeO_3$ (a) derived from the experimental loss function with **q**∥**c** using the Kramers-Kronig relations and (b) calculated within the Cu_5O_{12} cluster model.

suring technique (e.g., multiple reflection, surface effects) or can be ascribed to different qualities of the specimens under investigation (e.g., defects, impurities). However, the nonvanishing absorption in this energy range is responsible for the light blue gleam of the transparent single crystals of $CuGeO_3$ and thus its existence is beyond controversy. Above 2 eV, the energy position of the feature in σ_c derived from the KKA agree well with those from the optical measurements.

Furthermore, we calculated the current-current correlation function (which is proportional to the optical conductivity) with the polarization vector parallel to the **c** direction using the same model parameters as above. The results are shown in Fig. 6(b). The comparison with σ_c obtained from the experimental data illustrates the overall agreement and confirms the validity of the simplifying assumptions within our model described above.

Thus, our investigation of the loss functions (**q**∥**c**) and σ of $CuGeO_3$ below 7 eV can be summarized as follows.

(a) the EELS spectra as well as the optical conductivity can be described within a $(Cu3d_{x^2-y^2})_5(O2p_{x(y)})_{12}$ cluster model with a charge transfer energy $\Delta = 5.3$ eV, which is significantly higher than in other cuprates due to the larger difference in the Madelung potentials between the Cu and O sites.

(b) The features of the loss function have their origin in transitions into localized and delocalized final states which contribute to the signal in two well seperated energy regions above and below 4 eV, respectively.

(c) The increase of the NN coupling constant *x* leads to a shift of spectral weight from the high- to the low-energy region, as see experimentally for typical quasi-one-dimensional cuprates, such as Sr_2CuO_3.

(d) The intensity of the 1.8 eV feature in the optical conductivity derived from the loss function agrees well with results from optical absorption measurements described in Ref. 11. The analysis of our calculated loss function rules out the relation of this feature to charge transfer excitations between O $2p$ and Cu $3d$ states.

Having discussed the effects on the electronic structure of a chain of edge-sharing CuO_4 plaquettes generated by the variation of the interplaquette coupling we turn to the question whether the *d* electrons in $CuGeO_3$ actually possess either a quasi-one- or even higher-dimensional character. In this regard, the small distances between the Ge atoms and the O atoms of the CuO_2 chains (see Sec. II A) could provide an additional hopping path between adjacent chains. In order to study the mobility of the electrons along these paths we have carried out EELS measurements of $CuGeO_3$ with **q** parallel to the **b** direction. These results are discussed in the following section.

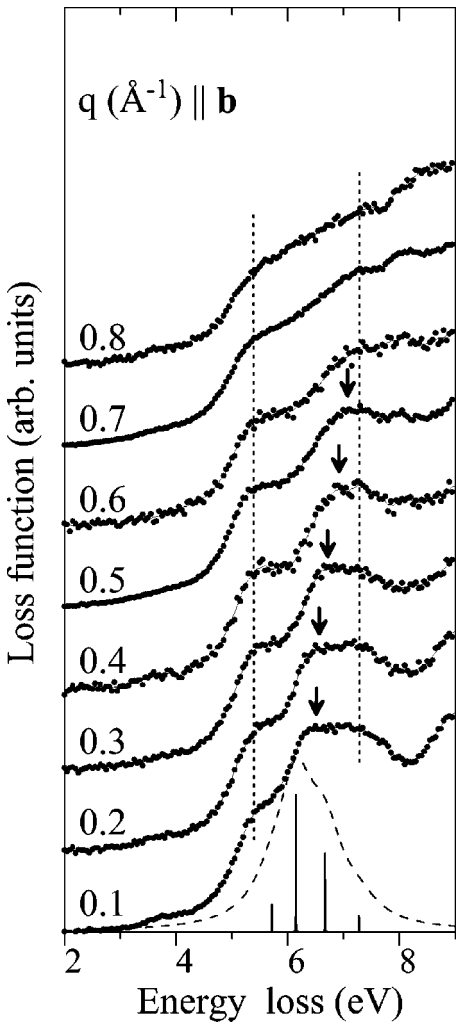

FIG. 7. Electron energy-loss spectra measured with momentum transfer parallel to the crystallographic **b** direction. For a comparison the dashed line and the solid vertical lines show the broadened (Gaussian function of 0.4 eV width) and unbroadened spectrum, respectively, for $\mathbf{q}_y = 0.1$ Å^{-1} where $\mathbf{q}_y$ is that component of **q**∥**b** which is aligned perpendicular to the chain axis in the plaquette plane. In the calculation we used the same Cu_5O_{12} cluster and the same parameter values as for the **c** direction. The vertical dotted lines illustrate the constant positions of the two shoulderlike features at 5.5 and 7.3 eV, while the arrows point out the dispersion of the 6.5 eV feature.

B. Loss function with q∥b

In Fig. 7 the energy dependent loss functions of $CuGeO_3$ for different momentum transfers parallel to the crystallographic **b** direction are shown. The spectra are normalized in

the manner described for $\mathbf{q}\|\mathbf{c}$. This allows a direct comparison between the absolute intensities of the spectra measured with the two different directions of the momentum transfer.

The shape of the loss functions with $\mathbf{q}\|\mathbf{b}$ differs strongly from those with $\mathbf{q}\|\mathbf{c}$, reflecting the anisotropy of the electronic structure in $CuGeO_3$. It is striking that below 4.5 eV almost no spectral weight is visible in the spectra. Due to dipole selection rules the NN and NNN hopping processes along the chain are strongly suppressed when the momentum transfer is aligned along the **b** direction. Thus, the lack of spectral weight for $\mathbf{q}\|\mathbf{b}$ in this energy range confirms the interpretation of the 3.5 eV peak in the spectra with $\mathbf{q}\|\mathbf{c}$ as coming from transitions into delocalized states as discussed in Sec. IV A. At first sight, the feature between 4.5 and 8 eV would seem to be composed of three interband plasmons. The plasmon excitation with the highest intensity at 6.5 eV is located between two shoulderlike features at 5.5 and 7.3 eV. The three plasmons show an interesting behavior with increasing momentum transfer. While the peak positions of the two shoulders remain constant (emphasized by the vertical dotted lines in Fig. 7) the plasmon at 6.5 eV appears to disperse by 0.5 eV between 0.1 and 0.5 Å^{-1} (marked by arrows in Fig. 7). Above 0.5 Å^{-1} it becomes rather difficult to distinguish between the dispersing feature and the plasmon at 7.3 eV as, with increasing **q**, the intensity of the first decreases faster than that of the latter.

With respect to the origin of the observed features, a theoretical analysis of the loss functions with $\mathbf{q}\|\mathbf{b}$ based on a cluster model is rather complicated because in this case the momentum transfer and the bonds between the atoms are not aligned within the same plane (see Fig. 1). If we assume that the interchain coupling along the **b** direction is negligible, then only intrachain excitations with $\mathbf{q}_y$ should contribute to the loss function, whereby $\mathbf{q}_y$ is the component of $\mathbf{q}\|\mathbf{b}$ aligned perpendicular to the chain axis in the plaquette plane. In this case a qualitative description of the loss function should be possible if we compare our experimental data with the loss functions calculated for different values of $\mathbf{q}_y$. The theoretical loss function using the same Cu_5O_{12} cluster and the same parameters as for the **c** direction is shown for $\mathbf{q}_y = 0.1$ Å^{-1} by the dashed curve in Fig. 7. The theoretical spectrum is composed of four plasmons whose positions lie in the energy range straddled by the experimental feature, illustrated by the corresponding unbroadened curve (vertical solid lines shown at the bottom of Fig. 7). However, it is clear that the distribution of the peak intensities does not reproduce the intensities observed in the experimental loss function. Furthermore, the ratios of the peak intensities in the theoretical spectra do not change significantly with increasing **q** (not shown), in contrast to the shift of spectral weight from 6.5 to 7 eV in the EELS spectra.

Figure 7 clearly indicates that our cluster model which yielded an excellent basis for the analysis of the valence band excitations in $CuGeO_3$ along the **c** direction, essentially fails to describe the loss functions in the **b** direction. This discrepancy leads to the conclusion that the interchain coupling via the Ge atoms is not negligible. Calculations of the band structure of $CuGeO_3$ show[6–8] that at around 3 eV above the chemical potential the Ge $4s$ and $4p$ states also contribute to a small extent to the DOS. Taking into account the strong overlap between the Ge orbitals and the $2p$ orbitals of the chain oxygens in the **b** direction, as well as the small angle of only about 35° between the Ge-O bonds and the direction of the momentum transfer for $\mathbf{q}\|\mathbf{b}$, presumably dipole transitions between the O $2p$ states—3 eV below the chemical potential—into the Ge $4s(p)$ states are the origin of additional spectral weight around 6–7 eV in the loss function. The strong dispersion of the Ge $4s$ final states would then explain the significant shift of the spectral weight to higher energies in the EELS spectra.

Consequently, a more detailed investigation of the loss function in the **b** direction requires a model which additionally takes into account the O-Ge-O paths between neighboring CuO_2 chains. Unfortunately, in suitable cluster models the cluster size for such an approach is currently too large for an exact diagonalization of the corresponding Hamiltonian matrix.

V. SUMMARY

In conclusion, we have presented a joint experimental and theoretical investigation of the valence band excitations of $CuGeO_3$. The momentum dependent loss functions of $CuGeO_3$ measured by means of EELS in transmission agree well with those obtained using a one-dimensional extended multiband Hubbard model at half filling. For the calculations we have used a cluster of five edge-sharing CuO_4 plaquettes. This model allowed us to determine the various transitions with $\mathbf{q}\|\mathbf{c}$ which contribute to the loss function below 7 eV. We found that the hole excitations contribute to the spectra in two well seperated energy regions each of them dominated by transitions into either localized (4–7 eV) or delocalized states (2–4 eV). With increasing interplaquette coupling, the spectral weight shifts from the high energy range to the low energy range as experimentally observed on going from quasi-zero-dimensional systems such as Li_2CuO_2 to one- or two-dimensional systems such as Sr_2CuO_3 and $Sr_2CuO_2Cl_2$. This shift of spectral weight to lower excitation energies in the materials with a more delocalized electronic structure is also connected to the spin interaction along the Cu-O chains (or in the Cu-O planes) which is ferromagnetic in Li_2CuO_2 and antiferromagnetic in $CuGeO_3$, Sr_2CuO_3, and $Sr_2CuO_2Cl_2$. In addition, from the EELS spectrum with $\mathbf{q} = 0.08$ Å^{-1} parallel to the **c** direction we have calculated the optical conductivity $\sigma_c(\mathbf{q},\omega)$ using the Kramers-Kronig relations. Above 2 eV σ_c agrees well with results from optical measurements. A peak with small intensity around 1.8 eV in the experimental spectrum is not reproduced by the calculated spectrum ruling out the assignment of this feature to charge transfer excitations between O $2p$ and Cu $3d$ states. We found an only qualitative agreement between the loss functions of $CuGeO_3$ with $\mathbf{q}\|\mathbf{b}$ and those calculated with momentum transfer perpendicular to the Cu_5O_{12} cluster

within the plaquette plane. However, an additonal dispersing feature which cannot be described within our cluster model can be observed between 6 and 7 eV. This feature can be most probably ascribed to transitions into Ge 4*s* and 4*p* final states and thus suggests the existence of an interchain hopping path mediated by the Ge atoms along the **b** direction.

ACKNOWLEDGMENTS

We thank L. Sangaletti for fruitful discussions. The calculations were performed on the Origin 2000 at the Technische Universität Dresden. Part of the work has been supported by the Deutsche Forschungsgemeinschaft under Contract No. DFG Fi-439/7-1.

[1] M. Hase, I. Terasaki, and K. Uchinokura, Phys. Rev. Lett. **70**, 3651 (1993).

[2] J.P. Pouget, L.P. Regnault, M. Ain, B. Hennion, J.-P. Renard, P. Veillet, G. Dhalenne, and A. Revcolevschi, Phys. Rev. Lett. **72**, 4037 (1994); K. Hirota, D.E. Cox, J.E. Lorenzo, G. Shirane, J.M. Tranquada, M. Hase, K. Uchinokura, H. Kojima, Y. Shibuya, and I. Tanaka, *ibid.* **73**, 736 (1994); M. Braden, G. Wilkendorf, J. Lorenzana, M. Ain, G.J. McIntyre, M. Behruzi, G. Heger, G. Dhalenne, and A. Revcolevschi, Phys. Rev. B **54**, 1105 (1996).

[3] E. Pytte, Phys. Rev. B **10**, 4637 (1974); L.N. Bulaevskii, A.I. Buzdin, and D.I. Khomskii, Solid State Commun. **27**, 5 (1978); M.C. Cross and D.S. Fisher, Phys. Rev. B **19**, 402 (1979); M.C. Cross, *ibid.* **20**, 4606 (1979).

[4] W. Geertsma and D. Khomskii, Phys. Rev. B **54**, 3011 (1996).

[5] J.B. Goodenough, Phys. Rev. **100**, 564 (1955); J. Kanamori, J. Phys. Chem. Solids **10**, 87 (1959); P.W. Anderson, Solid State Phys. **14**, 99 (1963).

[6] L.F. Mattheiss, Phys. Rev. B **49**, 14 050 (1994).

[7] Z.S. Popović, F.R. Vukajlović, and Z.V. Šljivančanin, J. Phys.: Condens. Matter **7**, 4549 (1995).

[8] H. Wu, M. Qian, and Q. Zheng, J. Phys.: Condens. Matter **11**, 209 (1999).

[9] Y. Mizuno, T. Tohyama, S. Maekawa, T. Osafune, N. Motoyama, H. Eisaki, and S. Uchida, Phys. Rev. B **57**, 5326 (1998).

[10] I. Terasaki, R. Itti, N. Koshizuka, M. Hase, I. Tsukada, and K. Uchinokura, Phys. Rev. B **52**, 295 (1995).

[11] M. Bassi, P. Camagni, R. Rolli, G. Samoggia, F. Parmigiani, G. Dhalenne, and A. Revcolevschi, Phys. Rev. B **54**, R11 030 (1996).

[12] S. Zagoulaev and I.I. Tupitsyn, Phys. Rev. B **55**, 13 528 (1997).

[13] F. Parmigiani, L. Sangaletti, A. Goldoni, U. del Pennino, C. Kim, Z.-X. Shen, A. Revcolevschi, and G. Dhalenne, Phys. Rev. B **55**, 1459 (1997).

[14] L.-C. Duda, J. Downes, C. McGuinness, T. Schmitt, A. Augustsson, K.E. Smith, G. Dhalenne, and A. Revcolevschi, Phys. Rev. B **61**, 4186 (2000).

[15] H. Völlenkle, A. Wittmann, and H. Nowotny, Monatsch. Chem. **98**, 1352 (1967).

[16] J. Fink, Adv. Electron. Electron Phys. **75**, 121 (1989).

[17] S.E. Schnatterly, Solid State Phys. **34**, 275 (1977).

[18] See, e.g., D. Pines, *Elementary Excitations in Solids* (Addison-Wesley, Reading, MA, 1963), Chaps. 3-4.

[19] R. Neudert, M. Knupfer, M.S. Golden, J. Fink, W. Stephan, K. Penc, N. Motoyama, H. Eisaki, and S. Uchida, Phys. Rev. Lett. **81**, 657 (1998).

[20] See, for example, H.Q. Lin and J.E. Gubernatis, J. Comput. Phys. **7**, 400 (1993), and references therein.

[21] J.C. Slater and G. Koster, Phys. Rev. **94**, 1498 (1954).

[22] L.F. Mattheiss, Phys. Rev. B **5**, 290 (1972).

[23] See, e.g., A.K. Mahan, R.M. Martin, and S. Satpathy, Phys. Rev. B **38**, 6650 (1988); M.S. Hybertsen, M. Schlüter, and N.E. Christensen, *ibid.* **39**, 9028 (1989); J.B. Grant and A.K. McMahan, *ibid.* **46**, 8440 (1992).

[24] V. Corradini, A. Goldoni, F. Parmigiani, C. Kim, A. Revcolevschi, L. Sangaletti, and U. del Pennino, Surf. Sci. **420**, 142 (1999).

[25] S. Atzkern, M. Knupfer, M.S. Golden, J. Fink, C. Waidacher, J. Richter, K.W. Becker, N. Motoyama, H. Eisaki, and S. Uchida, Phys. Rev. B **62**, 7845 (2000).

[26] F.C. Zhang and T.M. Rice, Phys. Rev. B **37**, 3759 (1988).